DESIGN OF A V-BAND HIGH-POWER SHEET-BEAM COUPLED-CAVITY TRAVELING-WAVE TUBE

Y. Liu[1],*, J. Xu[1], Y. Wei[1], X. Xu[1], F. Shen[1], M. Huang[1], T. Tang[1], W. Wang[1], Y. Gong[1], and J. Feng[2]

[1]National Key Laboratory of Science and Technology on Vacuum Electronics, School of Physical Electronics, University of Electronic Science and Technology of China, Chengdu 610054, China

[2]National Key Laboratory of Science and Technology on Vacuum Electronics, Beijing Vacuum Electronics Research Institute, Beijing 100015, China

Abstract—The design and analysis of a high-power wideband sheet-beam coupled-cavity traveling-wave tube operating at V-band is presented. The interaction circuit employs three-slot doubly periodic staggered-ladder coupled-cavity slow-wave structure, and a 5 : 1 aspect-ratio sheet electron beam is used to interact with the circuit. Combined with design of the well-matched input and output couplers, a 3-D particle-in-cell model of the sheet-beam coupled-cavity traveling-wave tube is constructed. The electromagnetic characteristics and the beam-wave interaction of the tube are investigated. From our calculations, this tube can produce saturated output power over 630 Watts ranging from 58 GHz to 64 GHz when the cathode voltage and beam current are set to 13.2 kV and 300 mA, respectively. The corresponding saturated gain and electron efficiency can reach over 32.5 dB and 15.9%. Compared with the circular beam devices, the designed sheet-beam TWT has absolute advantage in power capability, and also it is more competitive in bandwidth and electron efficiency.

1. INTRODUCTION

The V-band frequency range is a region of the millimeter-wave spectrum that has been developed mainly for inter-satellite communications [1]. As the key device, the amplifier critically determines the performance of the whole inter-satellite systems. Due

* Corresponding author: Yang Liu (yliu83@uestc.edu.cn).

to its outstanding combined performances in power capacity and bandwidth, traveling-wave tube (TWT) is one of the most important millimeter-wave amplifiers [2–9]. As a full-metal structure, coupled-cavity has been shown to have excellent performance in power capability. Consequently, there is considerable interest in the study and development of V-band coupled-cavity TWT. For example, Hughes-type coupled-cavity has been used to develop a 75 Watts, 59–64 GHz TWT [10]. With computer simulation, we also designed a 100 Watts, 58–62 GHz TWT by using the double-staggered ladder coupled-cavity structure [11]. However, both of them adopt the circular beam tunnel, the beam current will be restricted, and the maximum achievable power will be reduced as the beam tunnel size scale down.

In order to obtain higher power, the sheet electron beam has been considered for beam-wave interaction in coupled-cavity TWT. A novel coupled-cavity structure for high-power wideband millimeter-wave TWT, called sheet-beam coupled-cavity, is proposed by Simon J. Cooke etc. [12], as shown in Figure 1. The eigenmode calculations and linear small-signal analyses by Larsen et al. [13] show that this structure circuit has a significant gain and wide bandwidth when operating in Ka-band. Meanwhile, with the advent of modern computation, computer aided simulation has played an important role in the design and development of the TWT, which can significantly reduce the time and cost. Then, more and more engineers tend to perform simulation design before experimental study of the TWT [14–16]. In this paper, we will try to employ this novel structure to design a V-band TWT by means of computer simulation.

(a)   (b)
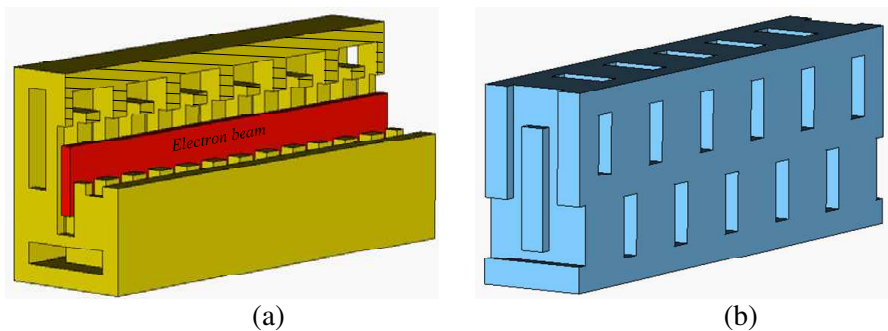
Figure 1. (a) Cutaway view of the three-slot doubly periodic staggered-ladder sheet-beam coupled-cavity solid model (with sheet-beam inserted in the beam channel). (b) The corresponding vacuum model in our simulation (the background material is metal).

The analysis and design of a V-band sheet-beam coupled-cavity TWT using Ansoft HFSS and CST studio suite [17–19] are presented here. In Section 2, the simulation model of the sheet-beam coupled-cavity structure is described in detail. High frequency properties such as dispersion characteristics, beam-wave interaction impedance are studied and optimized by HFSS. In Section 3, the input and output couplers are designed and the transmission characteristics of this circuit are obtained. In Section 4, a 3-D particle-in-cell model of the V-band sheet-beam coupled-cavity TWT is constructed. And the beam-wave interaction simulations are performed to predict the operating characteristics such as saturated output power, gain and electron efficiency. Section 5 concludes with a summary and description of future work.

2. SLOW-WAVE STRUCTURE DESIGN

Figure 2(a) shows the vacuum parameter model of the three-slot doubly periodic staggered-ladder sheet-beam coupled-cavity. The structure is derived from the double-staggered ladder coupled-cavity geometry [11, 20], and retains many of its desirable characteristics. An odd number of coupling slots connect consecutive rectangular
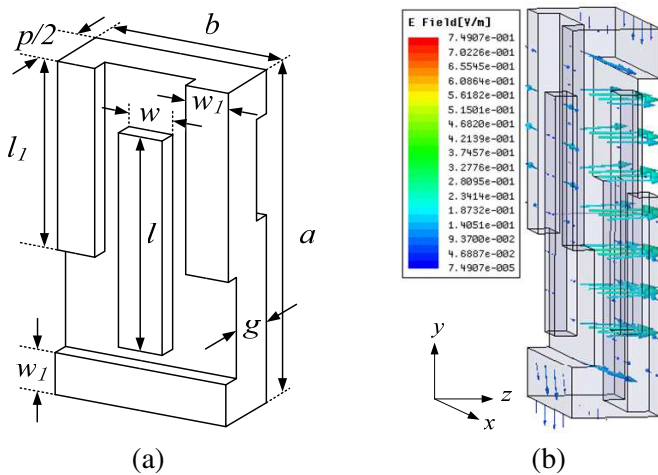
Figure 2. (a) Vacuum parameter model of the three-slot doubly periodic staggered-ladder sheet-beam coupled-cavity for one cell (half period). (b) Electric fields distribution of the fundamental mode with a phase shift near 1.5π.

cavities in the waveguide structure. The slots are distributed evenly around the periphery, including one slot along a side wall, and the pattern is alternated so that consecutive sets of slots are offset, as in the traditional double-staggered ladder structure [20]. For the remainder of this paper, the z-axis is in the direction of electron beam propagation (the axial direction), the y-axis is in the wide dimension of the structure, and the x-axis is in the short one.

Figure 2(b) plots the electric fields distribution of the fundamental mode (mode 1 in Figure 3(a)) for the sheet-beam coupled-cavity with a phase shift near 1.5π. The electric fields are mainly concentrated around the beam channel and have a predominant symmetric axial field distribution along the electron beam propagation direction, which is essential to beam-wave interaction of the TWT.

The high frequency properties of this structure were simulated by means of HFSS, which refer to the dispersion characteristics and beam-wave interaction impedance. Since the sheet-beam coupled-cavity is a periodic structure, the simulation can be carried out only in one pitch. And by employing master and slave boundary condition in the eigenmode solver [21], the simulation can be conducted and optimized in an efficient and accurate way. The typical optimized structural parameters are listed in Table 1. As investigated in detail by Paul B. Larsen etc. [13], this type of circuit is a fundamental backward wave circuit and the electron beam interacts with the first spatial harmonic, as shown in Figure 3(a). And an unconventional mode 2 appears in the dispersion diagram due to the introduction of wide sheet-beam channel. The normalized phase velocity versus frequencies of the fundamental
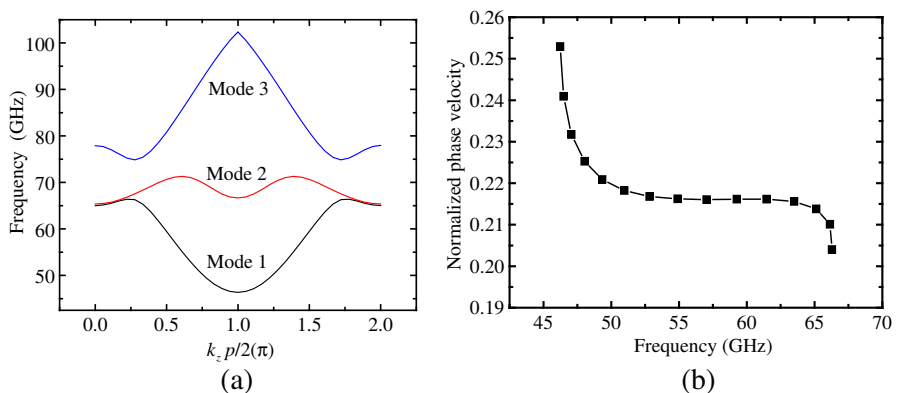
Figure 3. Dispersion curve of the three-slot doubly periodic staggered-ladder sheet-beam coupled-cavity.

Table 1. Parameters for the simulated SWS.

Parameter	Dimensions
Cavity $a \times b$	$3.57 \times 1.98 \, \text{mm}$
Cavity height (g)	$0.41 \, \text{mm}$
Slot 1 & 2 width (w_1)	$0.46 \, \text{mm}$
Slot 1 length (l_1)	$2.02 \, \text{mm}$
Slot 2 length	$1.98 \, \text{mm}$
Beam channel $(l \times w)$	$2.2 \times 0.44 \, \text{mm}$
Period length (p)	$1.64 \, \text{mm}$

mode at the first spatial harmonic is also given in Figure 3(b). It shows that the dispersion curve is quite flat over a broad bandwidth. And the phase velocity determines the beam voltage, approximately 13 kV, required for synchronized interaction with the electron beam.

As a measure of the interaction strength between the electron beam and RF wave, the average interaction impedance over the cross-section of the electron beam $(l/2 \times w/2)$ is also calculated by the field calculator in the eigenmode solver of HFSS, as shown in the insert of Figure 4. For calculating the average interaction impedance, we firstly need to divide the whole plane into small rectangular meshes. Then, it can be calculated by the following expression

$$K_{\text{average}} = \frac{\sum_1^n s_n K_n}{S} \tag{1}$$

where, s_n is the area of the nth mesh, K_n is the on-axis interaction impedance [22] defined on the center position of the nth mesh, and S is the whole area of the cross-section. If the area of each mesh is the same, the expression can be simplified as

$$K_{\text{average}} = \frac{\sum_1^n K_n}{n} \tag{2}$$

The denser is the chosen mesh, the more accurate are the calculation values. Here, we divide the plane into 400 (20×20) rectangular meshes. Then, by calculating the on-axis interaction impedance of each mesh (K_n), the average interaction impedance over the whole plane can be obtained by the formula (2), and the results are shown in Figure 4. Compared with the circular beam coupled-cavity structure, the impedance values are basically at the same level [11]. The sheet-beam can increase the beam power by distributing the beam
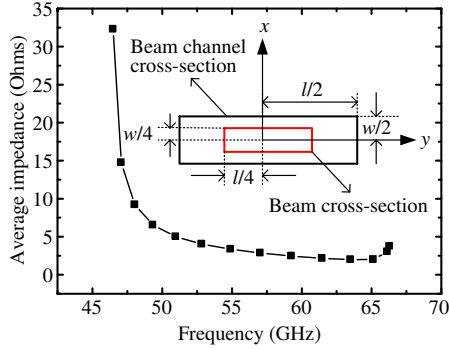
Figure 4. Average interaction impedance over the cross-section of the electron beam. (The right inset gives the cross-section view of the electron beam.).

current over an increased area, which indicates that the sheet-beam coupled-cavity TWT can obtain higher output power.

3. COUPLER DESIGN

A good coupler between the coupled-cavity circuit and the input/output waveguide is important for improving tube efficiency, gain and stability over the required bandwidth. It also helps in preventing the band-edge oscillation at the upper cut-off frequency of the cavity mode [23]. Therefore, the design and optimization of coupler for coupled-cavity is a very important work. However, coupled-cavity is inherently three-dimensional structure and the design of broadband, low-VSWR coupler is a complicated process. The available literatures on this aspect are relatively sparse and mainly limited to the circular beam structures [23, 24]. Furthermore, as sheet-beam coupled-cavity structures have more complex mode structure, designing a well-matched coupler would be more difficult.

Fortunately, a good design scheme for the sheet-beam coupled-cavity was proposed by Larsen et a. [25]. They designed an excellent coupler for ka-band sheet-beam coupled-cavity structure, which was also verified by experiments. Therefore, we mainly design the coupler for V-band sheet-beam coupled-cavity structure according to Larsen's scheme. As shown in Figure 5(a), the coupler is a three-stepped rectangular waveguide placed into the short edge of the input cavity. The narrow side length of the lowest rectangular waveguide is equal to the cavity height (g). Then, there are mainly five free parameters
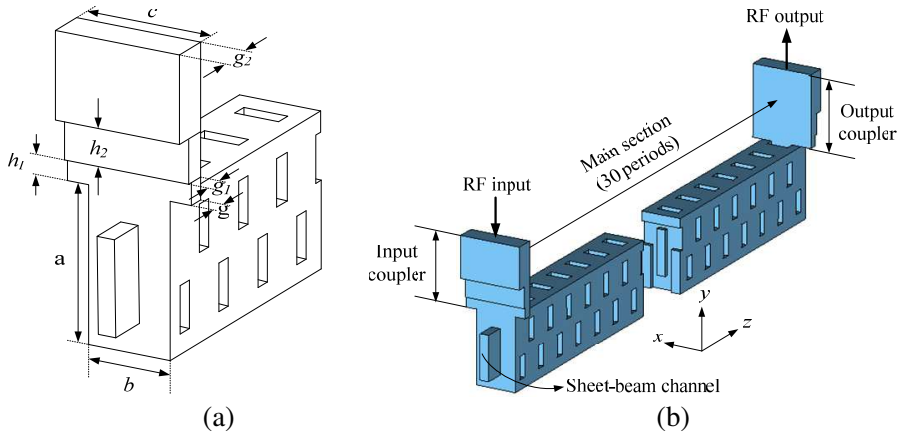
Figure 5. (a) Vacuum parameter model of the coupler. (b) The transmission vacuum model of the sheet-beam coupler-cavity circuit.

(c, g_1, g_2, h_1 and h_2) to be varied to optimize the VSWR within the range of interest. The transmission model of the sheet-beam coupler-cavity circuit including 25 periods of main section and input/output coupler is present, as shown in Figure 5(b). The boundary is set as copper with the effective conductivity of 3.5×10^7 S/m considering surface roughness [26, 27]. Using the transient solver in the CST Microwave Studio [18] and by sweeping the free parameters, the optimal coupler for sheet-beam coupled-cavity structure is obtained. The optimized parameters for the coupler and the simulated the transmission characteristics are given in Figure 6. The reflection parameter S_{11} is almost below -20 dB in the frequency range of 58–64 GHz. Together with the inset electric field distribution diagram, it demonstrates that the designed coupler is well matched to the sheet-beam coupled-cavity circuit over a wide frequency range.

4. BEAM-WAVE INTERACTION SIMULATIONS

In this section, a 3-D particle-in-cell model of sheet-beam coupled-cavity TWT is constructed. The beam-wave interaction simulations are carried out by using the PIC solver in CST Particle Studio [19] to substantiate the amplification capability of the TWT. As reflections caused by circuit discontinuities such as the mismatches between the input/output couplers and the SWS can cause oscillation, severs should be used to suppress these reflections [28]. Then, in order to obtain a large gain and suppress the oscillation, the whole interaction circuit is
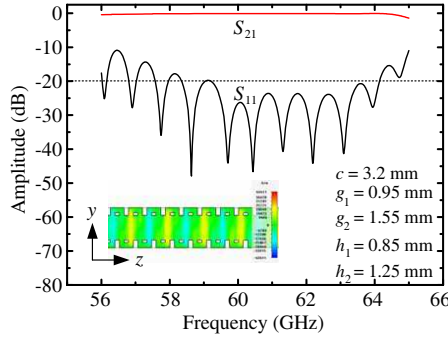
Figure 6. Transmission characteristics of the sheet-beam coupled-cavity circuit. (The lower left inset gives the z-component of electric field distribution at 61 GHz in the longitudinal section).
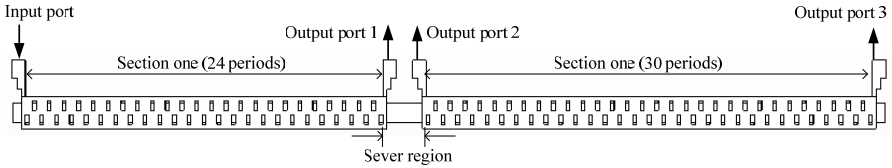
Figure 7. 3-D particle-in-cell vacuum model of the sheet-beam coupled-cavity TWT.

divided into two sections. The first section consists of 24 periods and the other 30 periods, as shown in Figure 7. Here, output port 1 and 2 are used as severs for suppressing the oscillation in our simulation. The dimensional parameters are listed in Table 1.

In the simulation, we assume that a sheet electron beam has a cross sectional area of $1.1 \times 0.22\,\mathrm{mm}^2$ ($l/2 \times w/2$, as shown in the inset of Figure 4) in the central area of the beam channel with $13.2\,\mathrm{kV}$ voltage and $300\,\mathrm{mA}$ current, corresponding to a beam aspect ratio of $5:1$ and beam filling factor of 25% with a current density of $124\,\mathrm{A/cm}^2$. And a uniform longitudinal magnetic field [29], with reasonable value of 0.6 Tesla, is used here to confine the sheet electron beam. The boundary is also specified as copper with the effective conductivity of $3.5 \times 10^7\,\mathrm{S/m}$.

The typical simulation results at the center frequency of 61 GHz are exhibited in Figures 8–14. As can be seen from the power transfer curve in Figure 8, when the input power is small, the output power increases linearly with the input power, that is to say, the tube operates
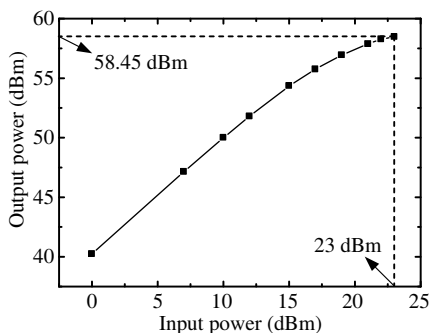
Figure 8. Power transfer curve at 61 GHz.
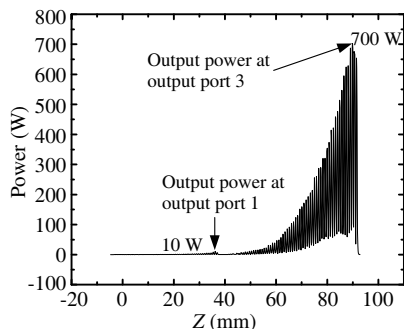
Figure 9. Growing wave plot as a function of the z-coordinate at 61 GHz.
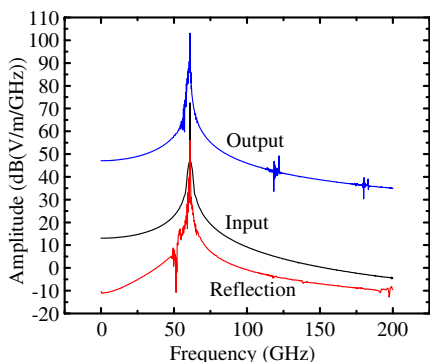
Figure 10. Frequency spectrum of input, output and reflected signals at 61 GHz.
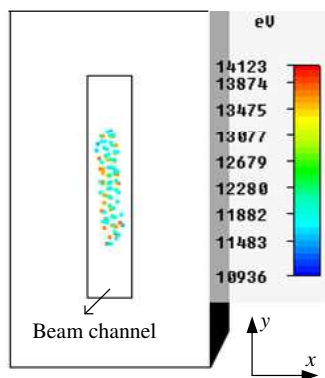
Figure 11. The cross-section view of the sheet electron beam at the end of the circuit.

in linear zone. But as the input power continues to grow, the tube will operate in nonlinear zone. When the input power increases to 200 mW (23 dBm), the tube can be driven up to saturated state with output power of 700 Watts (58.45 dBm), which can also be seen from Figure 9. Figure 10 gives the frequency spectrum of input, output and reflected signal. As for the output signal, the spectrum is relatively pure. Although the higher harmonics are also aroused, the amplitudes are much lower than that of the operating frequency of 61 GHz. Meanwhile, it can be learnt that the reflected power is well below the input power, which implies that the oscillation is unlikely to be occurred.

Figure 11 shows the cross-section view of the sheet electron beam at the end of the circuit. All of the electrons are well confined in the beam channel, with no electron intercepted. Figure 12 gives the electron bunching phenomenon around the end of the circuit. The accelerating electrons and retarding electrons are periodically arranged along the longitudinal direction, which demonstrates a good beam-wave energy exchange process. Figure 13 shows the phase momentum plot of the bunched electron beam along the longitudinal distance when the electron dynamic system has been in steady state. As the electron beam propagates along the circuit, most of electrons experience a continuous deceleration along the slow-wave circuit. This continuous interaction results in a continuously increasing wave amplitude at the output port of the TWT, as depicted in Figure 14. The power at output port 1 is 10 Watts, corresponding to the gain of 17 dB for the section one of the circuit. And the signal at output port 3 becomes stable at 700 Watts, without oscillation.
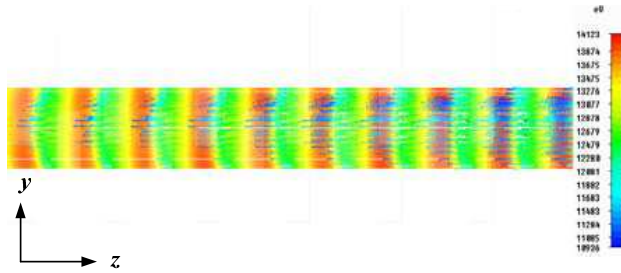
Figure 12. The electron bunching phenomenon at 61 GHz.
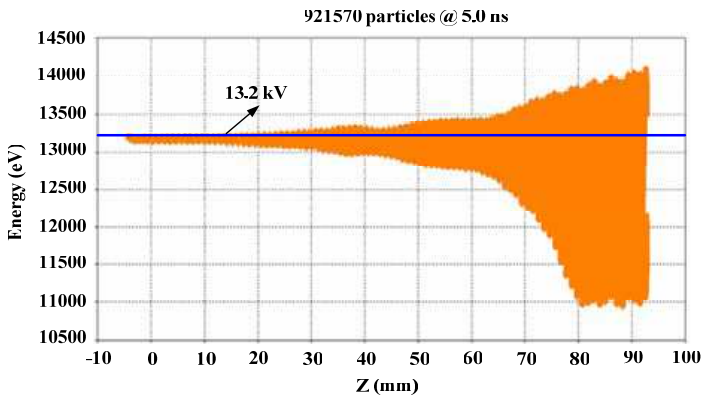
Figure 13. Phase momentum (p_z) plot of the bunched electron beam at 61 GHz.
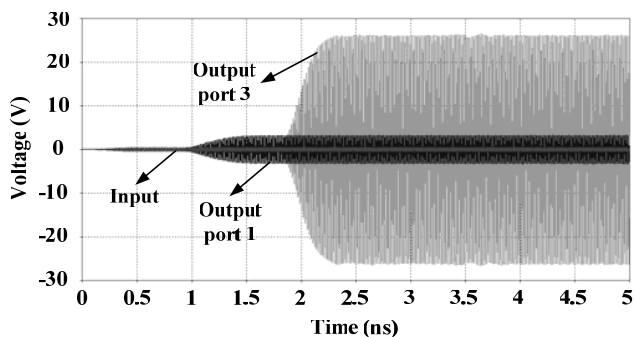
Figure 14. Input and output signals at 61 GHz.
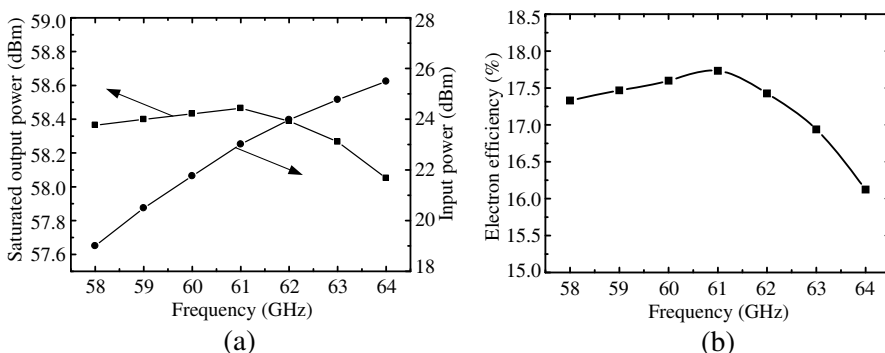
Figure 15. (a) The saturated output power versus input power plots cross the bandwidth of 58–64 GHz. (b) The saturated electron efficiency versus the frequency.

According to the same method, the TWT at each frequency can be driven to the saturated state by adjusting the input power. The saturated output power versus input power plots across the bandwidth of 58–64 GHz is shown in Figure 15(a). The designed sheet-beam coupled-cavity TWT can produce saturated output power of over 630 Watts (58 dBm) in the frequency range of 58–64 GHz, and the corresponding saturated gain can reach over 32.5 dB. The maximum saturated output power can reach 700 Watts at 61 GHz. Figure 15(b) gives the saturated electron efficiency versus the frequency, from which we can see that the saturated electron efficiency is greater than 15.9% across the bandwidth of 58–64 GHz.

Meanwhile, as the beam current density that we use here is relatively low ($124 \, \text{A/cm}^2$), the tube can obtain the higher output

power by increasing the current density. And also, the electron efficiency can be further improved by means of phase velocity tapers [30], which will be an important research subject for the sheet-beam coupled-cavity TWT.

5. CONCLUSIONS

The three-slot doubly periodic staggered-ladder coupled-cavity with sheet electron beam is employed in V-band traveling-wave tube. It is believed that this is the first time that 3-D particle-in-cell simulations have been conducted for a full-scale sheet-beam coupled-cavity traveling-wave tube. The simulation results show that the tube can produce a challenging output power over 630 Watts with a bandwidth of 6 GHz, and the corresponding gain and electron efficiency can reach over 32.5 dB and 15.9%. Compared with the circular beam devices, the performance of our designed sheet-beam TWT is more competitive. Therefore, it is a promising slow-wave structure for developing high-power, wideband and high efficiency millimeter-wave traveling-wave tubes. Future work will be concentrated on the electron optical system, especially on the formation, transmission and collection of the sheet electron beam. Also, the experiment study of this sheet-beam coupled-cavity TWT will be carried out.

ACKNOWLEDGMENT

REFERENCES

1. Kornfeld, G. K., E. Bosch, W. Gerum, and G. Fleury, "60-GHz space TWT to address future market," *IEEE Trans. Electron Devices*, Vol. 48, No. 1, Jan. 2001.
2. Kesari, V., "Beam-absent analysis of disc-loaded-coaxial waveguide for application in gyro-TWT (Part-1)," *Progress In Electromagnetics Research*, Vol. 109, 211–227, 2010.

3. Kesari, V., "Beam-present analysis of disc-loaded-coaxial waveguide for application in gyro-TWT (Part-2)," *Progress In Electromagnetics Research*, Vol. 109, 229–243, 2010.

4. Kesari, V. and J. P. Keshari, "Analysis of a circular waveguide loaded with dielectric and metal discs," *Progress In Electromagnetics Research*, Vol. 111, 253–269, 2011.

5. Mustafa, F. and A. M. Hashim, "Properties of electromagnetic fields and effective permittivity excited by drifting plasma waves in semiconductor-insulator interface structure and equivalent transmission line technique for multi-layered structure," *Progress In Electromagnetics Research*, Vol. 104, 403–425, 2010.

6. Mineo, M., A. Di Carlo, and C. Paoloni, "Analytical design method for corrugated rectangular waveguide SWS THz vacuum tubes," *Journal of Electromagnetic Waves and Applications*, Vol. 24, No. 17–18, 2479–2494, 2010.

7. Li, Z., J. H. Wang, F. Li, Z. Zhang, and M. Chen, "A new insight into the radiation mechanism of fast and slow traveling waves," *Journal of Electromagnetic Waves and Applications*, Vol. 25, No. 13, 1874–1885, 2011.

8. Shi, Z. J., Z. Q. Yang, F. Lan, G. Xi, F. Tao, and Z. Liang, "Investigation of a 30-GHz relativistic diffraction generator with a coaxial reflector," *Journal of Electromagnetic Waves and Applications*, Vol. 24, No. 17–18, 2453–2462, 2010.

9. Malek, F., "The analytical design of a folded waveguide traveling wave tube and small signal gain analysis using Madey's theorem," *Progress In Electromagnetics Research*, Vol. 98, 137–162, 2009.

10. Wilson, J. D., P. Ramins, and D. A. Force, "A high-efficiency 59 to 64 GHz TWT for intersatellite communications," *Proc. IEDM Tech. Dig.*, 585–588, 1991.

11. Liu, Y., Y. B. Gong, Y. Y. Wei, J. Xu, Z. Y. Duan, and W. X. Wang, "Design of a 100-W V-band coupled-cavity," *China-Japan Joint Microwave Conference (CJMW)*, 458–460, Hangzhou, China, 2011.

12. Cooke, S. J., B. Levush, and T. M. Antonsen, Jr., "A coupled-cavity slow-wave structure for sheet-beam devices," *Proc. IEEE Int. Vac. Electron. Conf.*, 487–488, Monterey, CA, 2006.

13. Larsen, P. B., D. K. Abe, S. J. Cooke, B. Levush, T. M. Antonsen, Jr., and R. E. Myers, "Characterization of a Ka-band sheet-beam coupled-cavity slow-wave structure," *IEEE Trans. Plasma Sci.*, Vol. 38, No. 6, 1244–1254, Jun. 2010.

14. Shin, Y. M., L. R. Barnett, and N. C. Luhmann, Jr., "Phase-shift traveling-wave-tube circuit for ultrawideband high-power submillimeter-wave generation," *IEEE Trans. Electron Devices*, Vol. 56, No. 5, 706–712, May 2009.

15. Han, S. T., K. H. Jang, J. K. So, J. I. Kim, Y. M. Shin, N. M. Ryskin, S. S. Chang, and G. S. Park, "Low-voltage operation of ka-band folded waveguide traveling-wave tube," *IEEE Trans. Plasma Sci.*, Vol. 32, No. 1, 60–66, Feb. 2004.

16. Kim, H. J., H. J. Kim, and J. J. Choi, "MAGIC3D simulations of a 500-W Ka-band coupled-cavity traveling-wave tube," *IEEE Trans. Electron Devices*, Vol. 56, No. 1, Jan. 2009.

17. Ansoft HFSS User's Reference, Ansoft Corp. [Online] Available: http://www.ansoft.com.cn/.

18. CST MWS Tutorials, CST Corp. [Online] Available: http://www.cst-china.cn/.

19. CST PS Tutorials, CST Corp. [Online] Available: http://www.cst-china.cn/.

20. James, B. G. and P. Kolda, "A ladder circuit coupled-cavity TWT at 80–100 GHz," *Proc. IEDM Tech. Dig.*, Vol. 32, 494–497, 1986.

21. Booske, J. H., M. C. Converse, C. L. Kory, C. T. Chevalier, D. A. Gallagher, K. E. Kreischer, V. O. Heinen, and S. Bhattacharjee, "Accurate parametric modeling of folded waveguide circuits for millimeter wave traveling wave tubes," *IEEE Trans. Electron Devices*, Vol. 52, No. 5, 685–693, May 2005.

22. Pierce, J. R., *Traveling-wave Tubes*, Van Nostrand, New York, 1965.

23. Christie, V. L., M. Sumathy, L. Kumar, and S. Prasad, "Optimization of waveguide coupler for coupled-cavity TWT using artificial neural network," *Proc. IEEE International Vacuum Electronics Conference (IVEC)*, 263–264, 2010.

24. Kageyama, T., "The design of the transition region in coupled-cavity TWT," *Proc. IEEE International Vacuum Electronics Conference (IVEC)*, 102–103, 2002.

25. Larsen, P. B., D. K. Abe, B. Levush, and T. M. Antosen, Jr., "Coupling a waveguide input to a sheet-beam coupled-cavity slowe-wave structure," *Proc. IEEE International Vacuum Electronics Conference (IVEC)*, 209–210, 2011.

26. Wilson, J. D. and C. L. Kory, "Simulation of cold-test parameters and RF output power for a coupled-cavity traveling-wave tube," *IEEE Trans. Electron Devices*, Vol. 42, No. 11, Nov. 1995.

27. Tischer, F. J., "Excess conduction losses at millimeter wavelengths," *IEEE Trans. Microw. Theory Tech.*, Vol. 24, 853–858, Nov. 1976.

28. Gilmour, A. S., Jr., *Principles of Traveling-Wave Tubes*, Artech House, Boston, MA, 1994.

29. Nguyen, K. T., J. A. Pasour, T. M. Antonsen, Jr., P. B. Larsen, J. J. Petillo, and B. Levush, "Intense sheet electron beam transport in a uniform solenoidal magnetic field," *IEEE Trans. Electron Devices*, Vol. 55, No. 5, 744–752, May 2009.

30. Wilson, J. D., "Design of high-efficiency wide-bandwidth coupled-cavity traveling-wave tube phase velocity tapers with simulated annealing algorithms," *IEEE Trans. Electron Devices*, Vol. 48, No. 1, Jan. 2001.